PHYSICAL REVIEW E **86**, 020901(R) (2012)

Nonequilibrium fluctuations of a remodeling *in vitro* cytoskeleton

Björn Stuhrmann,[1] Marina Soares e Silva,[1,*] Martin Depken,[2,†] Frederick C. MacKintosh,[2] and Gijsje H. Koenderink[1,‡]

[1]*Biological Soft Matter Group, FOM Institute for Atomic and Molecular Physics (AMOLF), Science Park 104, Amsterdam 1098 XG, The Netherlands*

[2]*Department of Physics and Astronomy, Vrije Universiteit, Amsterdam 1081HV, The Netherlands*

(Received 13 April 2012; published 23 August 2012)

Motor proteins actively contract the actin cytoskeleton of cells and thereby give rise to nonequilibrium fluctuations as well as changes in the architecture of the cytoskeleton. Here, we show, by video microrheology of a reconstituted cytoskeleton, that motors generate time-dependent nonequilibrium fluctuations, which evolve as the network is remodeled. At earlier times, the fluctuation spectrum is dominated by strong non-Gaussian fluctuations, which arise from large displacements. At later times, directed displacements are infrequent and finally disappear. We show that these effects are due to contractile coarsening of the network into large actin-myosin foci.

DOI: 10.1103/PhysRevE.86.020901 PACS number(s): 87.16.Ka, 87.16.dj

Living organisms operate far from thermodynamic equilibrium. The consumption and dissipation of chemical energy allows living matter to create and to maintain complex hierarchical order. A prime example of ordering driven by energy dissipation is cytoskeletal reorganization [1–5]. Molecular motors embedded in the cytoskeleton convert chemical energy into mechanical work by sliding filaments past each other. Elucidating network stresses and dynamics that emerge from the collective action of motors and filaments is essential for a physical understanding of cytoskeletal self-organization into functional architectures that drive cell functions, such as migration, division, and tissue morphogenesis [6,7]. However, the complexity of cells hampers the identification of physical principles of self-organization. Reconstituted model actin-myosin cytoskeletons have proven valuable for investigating stress generation of motor-driven networks. Experimental approaches [8–10] and related theories [11,12] focus on the nonequilibrium behavior of network fluctuations. However, these studies focused on systems which did not evolve over time and were homogenous. In contrast, myosin evidently has the capacity to reorganize actin networks dramatically, both *in vivo* [13] and *in vitro* [2–5,14,15]. Long-wavelength continuum hydrodynamic approaches, that model the cytoskeleton as an active polar gel, yield flow patterns qualitatively consistent with observed motor-induced remodeling [16,17]. So far, however, a microscopic understanding is lacking for the dynamics in more realistic physiological systems in which motors generate both reorganization and fluctuations at the same time. This requires experimental investigations that link nonequilibrium fluctuations to structural network evolution.

Here, we quantify the dynamics of myosin motor-driven actin networks as they actively remodel on time scales relevant to living cells. To measure dynamics on micron length scales, we use video particle microrheology of inert beads embedded in the network to serve as passive probes [8]. We perform ensemble-averaged particle fluctuation analysis and develop a new algorithm to segment individual particle trajectories into periods of random and directed motion. We show that network restructuring is reported by rare directed particle motion events, which give rise to strongly non-Gaussian statistics. By spectral analysis, we find that the time scale of active displacement fluctuations drops from 20 to 10 s within 40 min of sample evolution. We find a strong correlation between the observed dynamics and the structural evolution of the network, which we observe by microscopy. Our results provide a new direction for future theoretical modeling of motor-driven materials [11,12,16,17] and suggest a new approach towards the interpretation of microrheology in living cells [6,18].

Active cytoskeletal networks were reconstituted by polymerizing globular (G-)actin in the presence of bipolar myosin II motor filaments. Actin and myosin were purified from rabbit skeletal muscle [19,20]. Actin was stored in monomeric form at -80 °C in G-buffer [2 mM Tris-HCl, 0.2 mM adenosine triphosphate (ATP), 0.2 mM $CaCl_2$, 0.2 mM dithiothreitol (DTT), and 0.005% NaN_3, *p*H 8.0]. Myosin was stored at -20 °C in a high salt buffer (0.6 mM KCl, 1 mM DTT, 50 mM phosphate, *p*H 6.3, and 50% weight-to-weight ratio of glycerol) that preserves it in a nonprocessive monomeric form. Before experiments, myosin was dialyzed against 300 mM KCl, 4 mM $MgCl_2$, 1 mM DTT, and 25 mM imidazole at *p*H 7.4. To initiate the formation of processive myosin II filaments, the myosin solution was diluted with 25 mM imidazole buffer (*p*H 7.4) to 70 mM KCl where myosin forms filaments composed of ≈200 motors [21]. Actomyosin network formation was then initiated by mixing G-actin and myosin filaments at final concentrations of 23.8 and 0.12 μM, respectively, in 25 mM imidazole-HCl, 0.1 mM MgATP, 50 mM KCl, 2 mM $MgCl_2$, and 1 mM DTT (*p*H 7.4). Samples contained 2 mM Trolox to prevent photobleaching, and 1.25 mM creatine phosphate and 26 units/ml creatine to prevent ATP depletion [4]. Actin was fluorescently labeled by mixing in 5 mol % Alexa488-labeled G-actin, and each molecule of myosin was labeled with, on average, three molecules of DyLight-594 NHS-Ester (Perbio, Etten-Leur, The Netherlands) [4]. Actin filament cross-links were created by co-polymerizing actin with 0.1 mol % biotinylated G-actin and streptavidin in a molar ratio of 1:25 to actin.

*Present address: Developmental Biology Program, Sloan-Kettering Institute, 1275 York Avenue, New York, NY 10065.

†Present address: Department of Bionanoscience, Kavli Institute of Nanoscience, Delft University of Technology, Delft, The Netherlands.

‡gkoenderink@amolf.nl

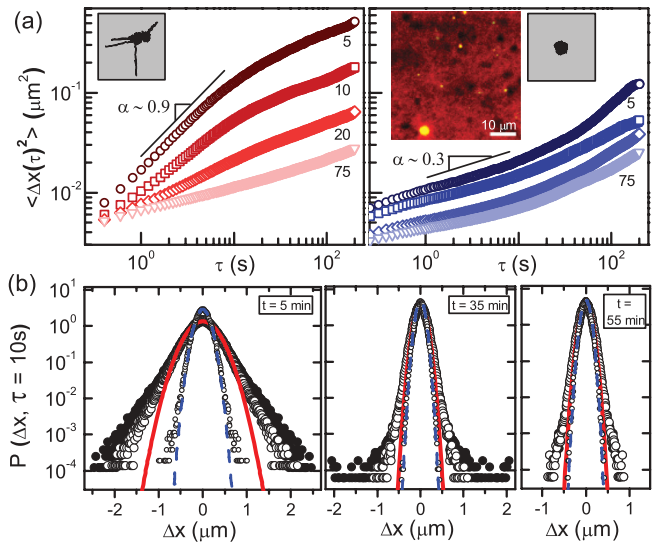

FIG. 1. (Color online) (a) Ensemble-averaged mean square displacements of probe particles in left: motor-driven *active* gels and in right: *passive* gels devoid of motors at different sample ages (indicated as numbers in minutes). Gray insets: example trajectories (box width 4 μm). Large inset: dark holes: homogenously distributed probe particles in an actin-myosin gel (red: actin; green: myosin). (b) Ensemble-averaged van Hove correlation functions of probe particles in large circles: active and small circles: passive gels for different sample ages t at lag time $\tau = 10$ s. Solid (dashed) line: Gaussian fit to active (passive) data. Large open circles indicate displacement probabilities after removal of directed motion events from particle trajectories.

Poly(L-lysine)-poly(ethylene glycol)-coated polystyrene microspheres (2 μm diameter) were added as inert tracers. Fluorescence microscopy of unlabeled spheres inside labeled actomyosin networks confirmed negligible accumulation of actin or myosin at the bead surfaces [inset in Fig. 1(a)]. G-actin was always added last, and the samples were then immediately transferred to custom-made glass flow chambers (25 μm height), closed with silicone grease, and directly observed by bright field microscopy. Flow cell surfaces were passivated with 0.1 mg/ml κ-casein. Video particle tracking was performed using custom-written software based on existing algorithms [22].

We first measure the dynamics of probe particles in samples devoid of motors, which we refer to as *passive*. The particle trajectories show purely random motion of small amplitude, consistent with thermal fluctuations [Fig. 1(a), right (small) inset]. By contrast, particle trajectories in motor-driven *active* networks exhibit large amplitude fluctuations along with episodes of clear directed motion (Fig. 1(a), left (small) inset; Supplemental Material [23]). To quantify the spatiotemporal characteristics of particle motion, we compute ensemble-averaged mean square displacements (MSDs) $\langle \Delta x(\tau)^2 \rangle \propto \tau^{\alpha}$, where τ represents lag time and α represents a diffusive exponent. Because we notice changes in the MSD over time, we divide the entire 80 min movie into bins of 5 min. MSDs in passive samples are characteristic of the subdiffusive behavior expected in weakly cross-linked gels [Fig. 1(a), right panel]. Indeed, rheology demonstrates weak solidlike behavior with a plateau elastic modulus of $G(\omega)' \approx 0.4$ Pa (Supplemental Material [23]). There is no significant dependence of the MSD on sample age. In the lag time window of 1–10 s, the diffusive exponent is $\alpha \approx 0.25$. In contrast, active networks show a striking change in the MSD as the sample ages [Fig. 1(a), left panel]. Initially, the MSD exhibits both a large amplitude and a large diffusive exponent $\alpha \approx 0.9$ for lag times between 1 and 10 s, reminiscent of diffusivelike behavior reported in cells [6,24] and *in vitro* cytoskeletons [10]. However, the magnitudes of the MSD and the diffusive exponent rapidly decrease and become indistinguishable from the MSD of passive networks after aging times of 40 min [Fig. 4(b)]. This is surprising since the motors continue to dissipate chemical energy as the ATP level is kept constant by enzymatic regeneration.

The MSD shows clear differences between active and passive networks, but the MSD alone is insufficient to distinguish between equilibrium and nonequilibrium effects. To test whether active fluctuations affect the ensemble averaged dynamics, we look, in addition, at the probability distribution of probe particle displacements as a function of lag time τ, $P(\Delta x,\tau)$, known as the van Hove correlation function [Fig. 1(b)]. For passive gels and at lag times that are in the network's elastic plateau regime (Supplemental Material [23]), Gaussian ensemble-averaged van Hove correlations are expected with only small deviations due to the heterogeneous cross-linking structure of F-actin networks [9,25]. Passive gels indeed show the anticipated Gaussian behavior, except during the first 5 min, which is likely due to initial rapid actin polymerization. A narrowing of van Hove correlations with time reflects a progressive increase in gel stiffness, consistent with rheological measurements (Supplemental Material [23]). For active gels, due to the contribution of nonequilibrium forces, no *a priori* reason exists for assuming Gaussian characteristics of particle motion. We find that the distributions of displacements for active samples deviate substantially from Gaussian [Fig. 1(b)]. They seem to be composed of a Gaussian contribution, which is broader than for passive networks, and marked tails.

To quantify the effect of motor activity on the Gaussian part of the van Hove functions, we compute the ratio β of active to passive widths as determined by Gaussian fits to the van Hove correlation functions. With motor activity, the width of the van Hove correlation functions can be affected both by stochastic motor stresses and by motor-induced stiffening of the networks. The former will tend to increase β, whereas, the latter will tend to decrease it. We observe active stiffening by a factor of up to 2.3 for all sample ages and lag times under investigation (Supplemental Material [23]). Any increase in β can, thus, be expected to represent an underestimate of the effects of active stress fluctuations. Gaussian broadening is seen to decrease monotonically over the course of sample evolution, reaching a plateau value $\beta \approx 1.2$ after 40 min of aging [Fig. 4(b)]. A spectral examination of van Hove correlations reveals that β depends on lag time and reaches a well-defined maximum at a lag time that depends on sample age [Fig. 2(a)]. At the beginning of sample evolution, this time scale is close to 20 s. It drops monotonously to approximately 10 s in the course of 40 min and then stays constant. These values are close to the crossover time of 10–30 s where the MSD has an inflection [Fig. 1(a)].

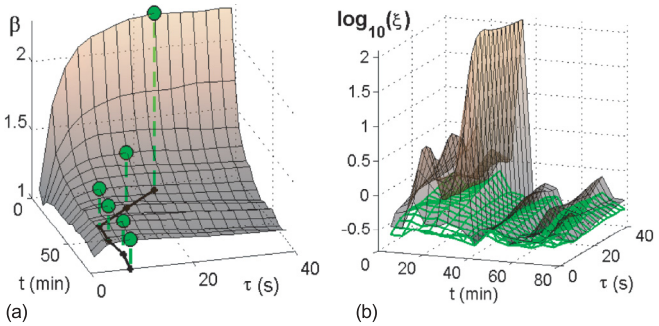

FIG. 2. (Color online) Quantification of active fluctuations as functions of sample age t and lag time τ. (a) Ratio of widths of Gaussian fits to ensemble-averaged van Hove correlation functions of active and passive samples. Circles: Maxima at given t. (b) Non-Gaussian parameter of van Hove correlation functions of active samples. Brown (upper) surface: original data. Green (lower) grid: data after removal of directed motion events from particle trajectories.

To quantify the effect of motor activity on the non-Gaussian part of the van Hove functions, we calculate the non-Gaussian parameter,

$$\xi = \frac{\langle \Delta x(\tau)^4 \rangle}{3\langle \Delta x(\tau)^2 \rangle^2} - 1, \tag{1}$$

which is zero for a Gaussian distribution [9]. Indeed, we observe near-zero values of ξ for passive networks, independent of lag time or sample age [Fig. 4(b)]. In contrast, active gels are characterized by large and highly fluctuating ξ values in the first 40 min of sample evolution [Fig. 2(b)]. After 40 min, ξ drops substantially and no longer fluctuates. Strong fluctuations in ξ with lag time prevent the identification of a distinct time scale of non-Gaussian activity. Nevertheless, the overall time scale is in agreement with values of $\sim$10 s obtained in actin-myosin networks by Toyota *et al.* [9]. Interestingly, actin-myosin networks that contain microtubules as force probes also show non-Gaussian fluctuations but on much shorter time scales of $\approx$0.1 s [10], which can be attributed to an ATP concentration that is 50-fold higher than in our system.

What is the origin of the pronounced tails of the van Hove functions? The observed periods of directed motion in active networks [Fig. 1(a), left (small) inset] naturally suggest an origin of the pronounced tails. To verify that the tails indeed reflect directed motion—and not network inhomogeneity—we developed a segmentation algorithm to distinguish periods of directed motion from periods of apparently random motion in individual particle trajectories (Fig. 3, Supplemental Material [23]). Similar to methods which extract motor-generated ballistic particle translocation from diffusive motion [26], we perform a local analysis of trajectory directionality and define directed motion events as sequences where frame-to-frame direction changes do not exceed $\pm 20^\circ$ for at least 0.8 s. Passive control samples do not show directed motion events using these parameters. Our algorithm allows us to calculate the probability of a particle to show directed motion p_{dir} as the ratio of the total time of detected directed motion to the total tracked time of all particles. Initially, this probability is close to 8%, but after 40 min, it has dropped to a constant

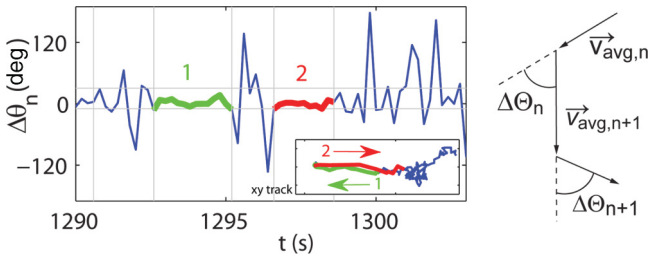

FIG. 3. (Color online) Left: thresholding of the frame-to-frame directional change $\Delta\Theta_n$ to retrieve time spans of directed motion shown for a short segment of a particle trajectory in an active gel. Right: Calculation of $\Delta\Theta_n$ from window averaged (window 1 s) velocity components.

value of 0.4% [Fig. 4(b)]. These segmentation results are sensitive to the choice of parameters. Increasing the minimum duration, for accepted directed motion events, from 0.8 to 1.0 s decreases p_{dir} by 40% at each sample age. However, the drop in p_{dir} to a constant low value within 40 min is conserved. By deleting the identified directed motion periods from the original trajectory data, we are able to largely remove the non-Gaussian contribution to the van Hove correlation functions, in particular, for intermediate sample ages between 10 and 40 min [Fig. 1(b)]. The non-Gaussian parameter drops to values close to that of passive networks [Figs. 2(b) and 4(b)]. The pronounced tails, thus, indeed originate from directed motion events. This operation demonstrates that only a minute fraction p_{dir} of tracked time gives rise to non-Gaussian tails, i.e., only very few events report essential system restructuring. As exemplified here, cytoskeletal systems which evolve rapidly on physiological time scales, will create new challenges for the development of testable models due to inherently low statistics.

As summarized in Fig. 4(b), all derived measures of nonequilibrium activity (α, β, ξ, and p_{dir}) show a striking decrease on a time scale of 40 min. To find the origin of this behavior, we correlate the activity measures with network structural reorganization, which we investigate by fluorescence microscopy [Fig. 4(a)]. We observe that myosin motors actively move within the initially homogenous network and coalesce into small foci in the first 10 min of sample evolution. After 10 min, the myosin foci start to change the network structure by locally condensing actin into a dense shell. Between 30 and 40 min, the network further coarsens by contractile coalescence of foci into large clusters. It is remarkable that microscopically polar motor activity gives rise to large-scale contractility in a disordered macroscopically apolar network. This contractility can be explained by the intrinsically asymmetric response of actin filaments to axial loading [4,27]. Clusters of myosin motors can randomly generate either tensile or compressive forces along the actin filaments. But only tensile forces can be supported by the high stretch modulus of actin filaments. Compressive forces, by contrast, are limited by the low threshold for buckling of actin filaments. Thus, forces mediated through the network can be expected to be almost exclusively tensile, which tend to drive contraction. This can explain both actin condensation around myosin foci and subsequent coalescence of myosin foci into larger clusters [4]. The correlated drop in the probability of directed motion p_{dir} and the diffusive exponent α coincide

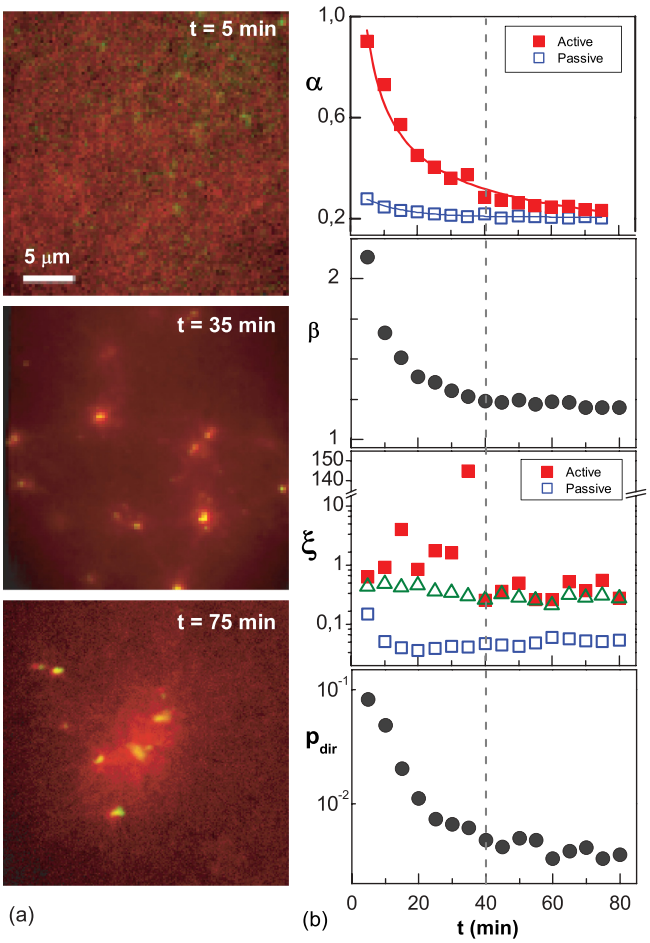

FIG. 4. (Color online) (a) Confocal fluorescence micrographs of an active actin-myosin gel, showing coarsening in three phases. The red: actin network and the green: myosin distribution are initially homogeneous ($t = 5$ min). Within 10 min, myosin filaments coalesce into foci. After 35 min, foci are surrounded by shells of condensed actin. After 75 min, actomyosin foci have coalesced into large clusters. (b) Multiple measures of nonequilibrium activity decay on a time scale of 40 min (see the Supplemental Material [23] for a sample-to-sample variability of results): from top to bottom, diffusive coefficient α, the Gaussian standard deviation ratio β, the non-Gaussian parameter ξ at lag time 10 s, and the probability for a particle to undergo directed motion p_{dir}. The dashed line indicates the transition to steady state. Triangles show ξ after removal of directed motion events.

with the observed restructuring period between 10 and 40 min. The non-Gaussian contributions ξ are high and highly fluctuating in the restructuring period. After 40 min, no mesoscale restructuring can be observed, and the system attains a stationary state where the active motors no longer rearrange the network. We hypothesize that only very few motors are left in the intervening network and that the motors in the foci are insulated by the locally condensed actin, preventing further actin condensation and coalescence of the foci. The non-Gaussian contributions ξ accordingly attain a steady-state value, which is close to that of passive samples.

Existing models of motor-driven networks either hydrodynamically describe the long-wavelength patterns of material flow [16,17] or describe fluctuations in a homogeneous network that does not evolve over time and that is interspersed with motors which spontaneously generate stresses [11,12]. In contrast, realistic cellular situations call for an amalgamation of both approaches. Our data encourage new modeling approaches by correlating signatures of activity with mesoscale structural properties of a dynamically arranging reconstituted cytoskeleton. With non-Gaussianity and elevated diffusive exponents, we reproduce features, which have previously been found in several tracking experiments *in vivo* [24,28–30] and *in vitro* [10]. Notably, our measures of nonequilibrium activity attain values of the passive samples once the network has reached a steady state, despite consistent motor activity. This indicates that, at late times, motor stresses are not efficiently transmitted through the network. Concomitantly, we observe a drop in the time scale of nonequilibrium particle amplitude fluctuations. This time scale has previously been measured only for networks in steady state [9,10]. In addition to correlations of structure and fluctuations, the second key result of this Rapid Communication is that the discontinuous dynamics of active systems that are heterogeneous, both in space and time, gives rise to inherently poor statistics. The van Hove tails in our experiments can be accounted for by very few, sometimes even single, contractile events. Our findings illustrate the necessity for a new approach towards the interpretation of microrheology in cells. First, bead ensemble analysis must be combined with the examination of individual trajectories. Extraction of directed motion events—as performed here—and correlation analyses thereof can access information, which has, so far, not been harvested from microrheological data, including length scales and (an)isotropy of stress propagation. Second, dynamics have to be carefully correlated with mesoscale structure. An important next step towards a deeper understanding of the complex interplay of stress generation and system restructuring is, furthermore, the mechanical characterization of *in vitro* systems by active (laser) microrheology [8]. The outlined approaches will help to better understand motor-driven networks, which are relevant to living cells and may provide inspiration for material science.

We thank S. Duineveld, M. Kuit-Vinkenoog, and I. Piechocka for help in protein purification and M. Seynen for tracking software implementation. This work is part of the research program of the Foundation for Fundamental Research on Matter (FOM), which is financially supported by the Netherlands Organization for Scientific Research (NWO). This work was financially supported by a VIDI grant from NWO, the European Union through Marie Curie Fellowship Grant No. PIEF-GA-2009-235258 (B.S.) and a Human Frontiers Young Investigator grant.

[1] F. J. Nédélec, T. Surrey, A. C. Maggs, and S. Leibler, Nature (London) **389**, 305 (1997).

[2] F. Backouche, L. Haviv, D. Groswasser, and A. Bernheim-Groswasser, Phys. Biol. **3**, 264 (2006).

[3] S. Köhler, V. Schaller, and A. R. Bausch, Nature Mater. **10**, 462 (2011).
[4] M. Soares e Silva, M. Depken, B. Stuhrmann, M. Korsten, F. C. MacKintosh, and G. H. Koenderink, Proc. Natl. Acad. Sci. USA **108**, 9408 (2011).
[5] D. Gordon, A. Bernheim-Groswasser, C. Keasar, and O. Farago, Phys. Biol. **9**, 026005 (2012).
[6] C. P. Brangwynne, G. H. Koenderink, F. C. MacKintosh, and D. A. Weitz, J. Cell Biol. **183**, 583 (2008).
[7] F. C. MacKintosh and C. F. Schmidt, Curr. Opin. Cell Biol. **22**, 29 (2010).
[8] D. Mizuno, C. Tardin, C. F. Schmidt, and F. C. MacKintosh, Science **315**, 370 (2007).
[9] T. Toyota, D. A. Head, C. F. Schmidt, and D. Mizuno, Soft Matter **7**, 3234 (2011).
[10] C. P. Brangwynne, G. H. Koenderink, F. C. MacKintosh, and D. A. Weitz, Phys. Rev. Lett. **100**, 118104 (2008).
[11] F. C. MacKintosh and A. J. Levine, Phys. Rev. Lett. **100**, 018104 (2008).
[12] D. A. Head and D. Mizuno, Phys. Rev. E **81**, 041910 (2010).
[13] C. A. Wilson, M. A. Tsuchida, G. M. Allen, E. L. Barnhart, K. T. Applegate, P. T. Yam, L. Ji, K. Keren, G. Danuser, and J. Theriot, Nature (London) **465**, 373 (2010).
[14] D. Smith, F. Ziebert, D. Humphrey, C. Duggan, M. Steinbeck, W. Zimmermann, and J. Käs, Biophys. J. **93**, 4445 (2007).
[15] P. M. Bendix, G. H. Koenderink, D. Cuvelier, Z. Dogic, B. N. Koeleman, W. M. Brieher, C. M. Field, L. Mahadevan, and D. A. Weitz, Biophys. J. **94**, 3126 (2008).
[16] T. B. Liverpool and M. C. Marchetti, Phys. Rev. Lett. **90**, 138102 (2003).
[17] K. Kruse, J. F. Joanny, F. Jülicher, J. Prost, and K. Sekimoto, Phys. Rev. Lett. **92**, 078101 (2004).
[18] B. D. Hoffman, G. Massiera, K. M. Van Citters, and J. C. Crocker, Proc. Natl. Acad. Sci. USA **103**, 10259 (2006).
[19] S. S. Margossian and S. Lowey, Methods Enzymol. **85**, 55 (1982).
[20] J. D. Pardee and J. A. Spudich, Methods Enzymol. **85**, 164 (1982).
[21] J. F. Koretz, Methods Enzymol. **85**, 20 (1982).
[22] J. C. Crocker and D. G. Grier, J. Colloid Interface Sci. **179**, 298 (1996).
[23] See Supplemental Material at http://link.aps.org/supplemental/10.1103/PhysRevE.86.020901 for a movie of directed motion of probe particles, rheological data on bulk networks, details on the algorithm for the extraction of particle directed motion events, sample-to-sample variability of results, and for more information on the Supplemental Material.
[24] P. Bursac, G. Lenormand, B. Fabry, M. Oliver, D. A. Weitz, V. Viasnoff, J. P. Butler, and J. J. Fredberg, Nature Mater. **4**, 557 (2005).
[25] M. T. Valentine, P. D. Kaplan, D. Thota, J. C. Crocker, T. Gisler, R. K. Prud'homme, M. Beck, and D. A. Weitz, Phys. Rev. E **64**, 061506 (2001).
[26] D. Arcizet, B. Meier, E. Sackmann, J. O. Rädler, and D. Heinrich, Phys. Rev. Lett. **101**, 248103 (2008).
[27] M. Lenz, T. Thoresen, M. L. Gardel, and A. R. Dinner, Phys. Rev. Lett. **108**, 238107 (2012).
[28] I. M. Kulić, A. E. X. Brown, H. Kim, C. Kural, B. Blehm, P. R. Selvin, P. C. Nelson, and V. I. Gelfand, Proc. Natl. Acad. Sci. USA **105**, 10011 (2008).
[29] N. Gal and D. Weihs, Phys. Rev. E **81**, 020903(R) (2010).
[30] J.-H. Jeon, V. Tejedor, S. Burov, E. Barkai, C. Selhuber-Unkel, K. Berg-Sørensen, L. Oddershede, and R. Metzler, Phys. Rev. Lett. **106**, 048103 (2011).